JOURNAL OF PROPULSION AND POWER
Vol. 13, No. 3, May–June 1997

Improvements to Steady-State Combustion Modeling of Cyclotrimethylenetrinitramine

Jeffrey E. Davidson* and M. W. Beckstead†
Brigham Young University, Provo, Utah 84602-4100

Many improvements have been made to models of cyclotrimethylenetrinitramine combustion in the past few years. The one-dimensional model presented in this paper models the solid, two-phase, and gas regions using complex kinetics and concentration- and temperature-dependent thermophysical properties. Calculated values agree well with experimentally determined burning rate σ_p, melt layer thickness, surface temperature, and species concentration profiles. When including laser-assisted burning in the model, a dark zone appeared that was similar to that seen experimentally. With the laser-assisted case, the chemistry controlling the burning rate is significantly different from cases without the laser heat flux. Calculations show that the melt-layer thickness is determined primarily by the liquid thermal conductivity and the surface temperature is controlled by the vapor pressure correlation. All other model predictions are relatively insensitive to these parameters. The condensed-phase decomposition and evaporation/condensation submodel are the weakest areas of the model.

Nomenclature

A = pre-exponential rate constant
area = cross-sectional area, cm^2, with subscript l–g, area of liquid–gas interface
C = molar concentration, mole/cm^3
c_p = heat capacity, erg/g K
E_a = activation energy, cal/mole
H = molar enthalpy, erg/mole
h = specific enthalpy, erg/g
kk = number of gas-phase species
$\dot{m}$ = mass flow rate, g/s
n = number of bubbles per volume, 1E13 bubbles/cm^3
p = pressure
q = rate of progress variable, mole/cm^3 s
R = universal gas constant
r_b = burning rate, cm/s
s = sticking factor
T = temperature, K
u = gas velocity, cm/s
V = diffusion velocity, cm/s
v = velocity of liquid or gas in two-phase region, cm/s
W = molecular weight, g/mole
$\bar{W}$ = average molecular weight, g/mole
$\dot{w}$ = molar rate of production, mole/cm^3 s
X = mole fraction
x = distance from two-phase-gas interface, cm
Y = mass fraction
β = temperature exponent rate constant
γ = stoichiometric coefficient
λ = heat capacity, erg/cm s K
ρ = density, g/cm^3
σ_p = temperature sensitivity, 1/K
τ = dT/dx, K/cm
ϕ = void fraction

Subscripts
evap = evaporation
g = gas
gl = gas–liquid mixture
i = reaction i
init = initial
k = species k
l = liquid
l-g = liquid–gas interface
melt = melting
s = solid
$s-$ = just below liquid–gas interface
$s+$ = just above liquid–gas interface

Presented as Paper 96-0885 at the AIAA 34th Aerospace Sciences Meeting and Exhibit, Reno, NV, Jan. 15–18, 1996; received Feb. 8, 1996; revision received Dec. 27, 1996; accepted for publication Dec. 30, 1996.

*Graduate Student, Department of Chemical Engineering, 350 CB BYU.

†Professor, Department of Chemical Engineering. Associate Fellow AIAA.

Introduction

CYCLOTRIMETHYLENETRINITRAMINE (RDX) combustion has been the focus of much research over the past two decades. It is hoped that by thoroughly understanding and accurately modeling this monopropellant, a model and kinetic mechanisms can be established that could be extended to other propellants for a priori calculations. A brief summary of progress in nitramine modeling is given. Ben-Reuven et al.[1] modeled RDX combustion in three regions (solid, liquid, and gas). The kinetics were very global, but they were able to show good agreement (or at least the correct trends) between their model's predictions and experimental data. Ermolin et al.[2] used a detailed elementary-step mechanism to model the gas phase only. Their predicted species concentration profiles agreed very well with experimental results at 0.5 atm. Hatch[3] used a similar mechanism for cyclotetramethylenetetranitramine (HMX) combustion, but linked it to a condensed-phase model. He assumed that HMX decomposed in the condensed phase via two paths, but this model failed to give the correct burning rate vs pressure correlation. Melius[4] modeled RDX ignition with a detailed gas-phase mechanism. His condensed phase and burning rate calculations were dominated by an evaporation/condensation model. Yetter et al.[5] have made many additions and improvements to Melius' mechanism.[4] Their RDX gas-phase mechanism has been used in almost all subsequent RDX models that include elementary reactions. Liau and Yang[6] modeled RDX steady-state combustion in three regions (solid, two-phase, and gas). The condensed-phase mechanism included three subsurface reactions and evaporation. Hanson-Parr and Parr[7] published experimental results of laser-assisted RDX

combustion, which showed a two-flame structure separated by a dark zone that had not appeared without the laser assist. Ben-Reuven et al.[1] and Bizot et al.[8] showed dark zones in their models with global mechanisms, but were not considering any laser assist. Li and Williams[9] assumed no RDX decomposition in solid or liquid regions and assumed that a dark zone controls the burning rate. They included more steps in the primary flame zone to be compatible with their assumptions. However, based on experimental data, there should not be a dark zone unless there is a laser spreading out the flame. Other models that included detailed kinetic mechanisms have failed to show a dark zone. A recent model by Prasad et al.[10] has shown a dark zone under laser-assisted conditions. The current model considers the solid, two-phase (liquid and gas), and gas regions of the flame with and without laser assist. The purpose of this paper is to 1) describe the computer model in detail, 2) discuss the model inputs, and 3) demonstrate that the model does a reasonably good job in predicting and explaining experimental data.

Model Description

A general, one-dimensional steady-state solid propellant combustion model has been developed at Brigham Young University. It has been written to handle any monopropellant, but this paper presents the results on RDX only. The model divides RDX combustion into three regions: solid, melt layer (liquid and gas), and gas. The mass flow rate $\dot{m}$ is an eigenvalue of the problem and is determined by iteration by matching boundary conditions at the liquid–gas interface.

Solid Region

In the solid region it is assumed that the propellant does not decompose, which has also been assumed in many other models.[1,3,4,6] Only the energy equation is solved for this region

$$\rho r_b c_p \frac{dT}{dx} - \lambda_s \frac{d^2T}{dx^2} = 0 \tag{1}$$

with boundary conditions

$$T(-\infty) = T_{\text{init}}, \qquad T(0) = T_{\text{melt}} \tag{2}$$

Assuming constant c_p and λ, this equation can be solved

$$T(x_s) = T_{\text{init}} + (T_{\text{melt}} - T_{\text{init}})\exp[(\rho r_b c_p/\lambda_s)x_s] \tag{3}$$

Because r_b is part of the eigenvalue of the problem, the solid region cannot be solved until the rest of the problem is converged; therefore, the solid region calculations and their results do not affect the calculations in the rest of the model.

Liquid-Gas Two-Phase Region

Once the propellant melts several things can start happening. The propellant can evaporate or decompose into gas and/or liquid fragments creating a frothy melt layer. As a gas phase develops in this two-phase region, bubbles form. The approach followed in this model for the two-phase region is very similar to that taken by Liau and Yang.[6] The bubbles are represented by the void fraction (ϕ, the fraction of the original propellant liquid volume that has been converted to gas by either evaporation or decomposition). As in many models[6,10] mass diffusion is neglected in this two-phase region. Because the melt-layer thickness and the right boundary conditions are unknown until the solution is complete, the energy and species equations are treated as a system of initial boundary-value problems and solved using DVODE [a variable coefficient ordinary differential equation (ODE) solver].[11] The second-order energy equation

$$\dot{m}\frac{dT}{dx} - \frac{1}{c_{p,\text{gl}}}\frac{d}{dx}\left[\lambda(\text{area})\frac{dT}{dx}\right] + \frac{(\text{area})}{c_{p,\text{gl}}}\sum_{k=1}^{\text{no. of species}} \dot{w}_k H_k = 0 \tag{4}$$

is treated as two first-order ODEs

$$\frac{d}{dx}[\lambda(\text{area})\tau] = \dot{m}\tau c_{p,\text{gl}} + (\text{area})\sum_{k=1}^{\text{no. of species}} \dot{w}_k H_k \qquad \frac{dT}{dx} = \tau \tag{5}$$

The void fraction is calculated by keeping track of the volume of liquid changing to gas [Eq. (6)]. The model assumes that the liquid density is a function of temperature but not composition:

$$\frac{d(1-\phi)}{dx} = \frac{1}{\rho_l v_l}\sum_{k=1}^{\text{no. of liquid species}} \dot{w}_k \tag{6}$$

The steady-state equation for liquid species k (neglecting mass diffusion) is

$$\frac{d}{dx}[(1-\phi)\rho_l v_l Y_{l,k}] = \dot{w}_k \tag{7}$$

Likewise for the gas species

$$\frac{d}{dx}(\phi\rho_g v_g Y_{g,k}) = \dot{w}_k \tag{8}$$

The mass fractions (Y_l and Y_g) are the mass fractions in the liquid in the two-phase region and the mass fractions in the gaseous bubbles in the two-phase region, respectively (i.e., the sum of $Y_{l,i}$ equals 1.0 as does the sum of $Y_{g,i}$). Gas transport and thermodynamic properties are calculated via Chemkin[12] and Transport[13] subroutines. Liquid properties are mass averaged and calculated from temperature-dependent correlations discussed later. For the two-phase mixture, heat capacity is mass averaged and thermal conductivity is volume averaged.

Mass is conserved by incorporating

$$\dot{m}/\text{area} = \phi\rho_g v_g + (1-\phi)\rho_l v_l \tag{9}$$

into the subroutine that separates the variables in Eqs. (7) and (8) (ρ_g, ρ_l, v_g, v_l, $Y_{g,k}$, and $Y_{l,k}$). Two more assumptions are necessary before these variables can be separated. We assume $T_g = T_l$ and assume that v_l equals the surface regression rate (r_b),[6,14] which simplifies the mass conservation equation [Eq. (8)] to $\rho_g v_g = \rho_l v_l = \dot{m}/\text{area}$.

Reaction rates must be handled with caution because of the two-phase interactions. The volumetric species mass production rate $\dot{w}_i$ is calculated by

$$\dot{w}_k = W_k \sum_{i=1}^{\text{no. of rxns}} \gamma_{k,i} q_{i,k} \tag{10}$$

where the definition of the rate-of-progress variable $q_{i,k}$ depends upon the type of reaction. Reactions involving condensed-phase reactants are assumed irreversible. For reactions involving only liquid reactants ($fF + gG \rightarrow$ products):

$$q = AT^{\beta}\exp(-E_a/RT)X_F^f X_G^g(1-\phi) \tag{11}$$

For reactions involving only gas-phase reactants, the reactions can be reversible and the rate of progress variables are calculated by Chemkin subroutines.[12] The rate-of-progress variables are then multiplied by ϕ. Evaporation rates are treated as in Liau and Yang[6]:

$$q_{\text{evap}} = \text{area}_{\text{l-g}} \cdot s\left(\tfrac{1}{4}\sqrt{8RT/\pi W}\right)(pW/RT)[(p_{\text{vap}}/p) - X] \tag{12}$$

where X is the mole fraction of the species in the bubbles if calculating below the interface or in the gas region if calcu-

lating at the interface. Following Liau and Yang,[6] the area in Eq. (9) is a function of void fraction:

$$\text{area}_{l\text{-}g} = \begin{cases} (36\pi n)^{1/3}\phi^{2/3} & \phi < 1/2 \\ (36\pi n)^{1/3}(1-\phi)^{2/3} & \phi > 1/2 \\ 1 & \text{at surface} \end{cases} \tag{13}$$

For reactions involving a gas-phase species F attacking a liquid-phase species G, q is calculated by

$$q = \text{area} \cdot A T^{\beta} \exp(-E_a/RT) C_F^f X_G^g \tag{14}$$

(Note: for the RDX mechanisms presented in this paper, none of the reactions are of this last type.)

The initial boundary conditions are

$$\phi = 0, \qquad T = T_{\text{melt}}$$

$$\tau = \frac{\dot{m}}{\lambda_l}\left[\frac{\Delta H_{\text{melting}}}{W_{\text{propellant}}} + c_{p,s1}(T_{\text{melt}} - T_{\text{init}}) + \frac{c_{p,s2}}{2}(T_{\text{melt}}^2 - T_{\text{init}}^2)\right] \tag{15}$$

where $Y_{g,k} = 0$ for all gas species; $Y_{l,k} = 0$ for all liquid species except the monopropellant; and $Y_{l,\text{propellant}} = 1$. $\tau\lambda_l/\dot{m}$ is the energy required to heat the solid propellant from its initial temperature to its melting temperature.

The system of ODEs describing the two-phase region are integrated in x until a surface condition is reached. The program user may specify one of three conditions that will halt the two-phase calculations and call the last node the surface. These are 1) a specified surface temperature, 2) a specified surface void fraction, or 3) for condensed mechanisms involving evaporation, the location where the liquid mass flux times area is equal to the rate of evaporation [Eq. (16)]: $(1-\phi)\rho_l v_l \cdot \text{area} = q_{\text{evap}}$. Condition 1 can be used when experimentally determined T_s data exist (e.g., see Ref. 10). Condition 2 can be used with a specified void fraction of 1.0 for propellants that do not have a significant vapor pressure. Using condition 3, as done by Liau and Yang,[6] will give calculated values of T_s and surface void fraction. Once the surface is reached, any remaining liquid is mathematically evaporated (i.e., assumed to vaporize instantaneously). The surface temperature and mass flux fractions serve as boundary conditions for the gas region. Because RDX has a significant vapor pressure the third option was used for the calculations in this paper.

Gas Region

The gas region calculations are handled by a modified version of PREMIX[15] in the burner-stabilized mode. The modifications are minor and are not important enough to discuss. The equations describing the gas phase are

$$\dot{m} = \rho u(\text{area}) \qquad \rho = \frac{p\bar{W}}{RT}$$

$$\dot{m}\frac{dT}{dx} - \frac{1}{c_p}\frac{d}{dx}\left[\lambda(\text{area})\frac{dT}{dx}\right] + \frac{\text{area}}{c_p}\sum_{k=1}^{kk}\rho Y_k V_k c_{p_k}\frac{dT}{dx} + \frac{\text{area}}{c_p}\sum_{k=1}^{kk}\dot{w}_k h_k W_k = 0$$

$$\dot{m}\frac{dY_k}{dx} + \frac{d}{dx}[\rho(\text{area})Y_k V_k] - (\text{area})\dot{w}W_k = 0 \quad (k = 1, \ldots, kk) \tag{16}$$

This system of equations is solved using finite difference discretization and Newton's method. The solution is first converged on a coarse grid and then the grid is refined to obtain the resolution desired. Further details can be found in Ref. 15.

The model calculates the energy balance error in the gas region as enthalpy$_{\text{in}}$ minus enthalpy$_{\text{out}}$:

$$\dot{m}\bar{H}\big|_{\text{in}} = \lambda\left.\frac{dT}{dx}\right|_{l\text{-}g} + \dot{m}\bar{H}\big|_{\text{out}} \tag{17}$$

If the enthalpy flux error is greater than about 5% at low pressures and greater than 1% at high pressures (~100 atm), the model failed to accurately predict the adiabatic flame temperature. To reduce this error, the grid in the gas region must be refined.

Determining the Mass Flux

The eigenvalue $\dot{m}$ is determined by iteration between the two-phase and gas region calculations. The correct $\dot{m}$ will satisfy the energy balance at the two-phase/gas interface:

$$\lambda_{\text{gl}}\left.\frac{dT}{dx}\right|_{s-} + [\rho_l v_l(1-\phi)\Delta H_{\text{vap}}]_{s-} = \lambda_g\left.\frac{dT}{dx}\right| + q_{\text{laser}} \tag{18}$$

Equation (18) says that the heat flux back from the gas-phase flame and any laser heat flux must equal the heat flux into the gas phase plus the energy flux required to vaporize any remaining liquid. The laser flux is assumed to be absorbed at the surface. The solution procedure is as follows:

1) Specify propellant initial temperature, pressure, and a guessed $\dot{m}$.
2) Solve two-phase region equations.
3) Solve gas region equations, initially with a coarse grid.
4) Compare left and right sides of Eq. (18). If the heat flux balance error is less than tolerance, go to step 6. If the right side is greater than the left side decrease $\dot{m}$, or else increase $\dot{m}$. The first time this step is performed $\dot{m}$ is changed by a small percentage (~3%). On future steps the next $\dot{m}$ is determined by linear extrapolation based on the previous two $\dot{m}$. If the new $\dot{m}$ is drastically different from the previous $\dot{m}$ (≥30%), then a small change in $\dot{m}$ is made to get a better extrapolation.
5) Go to step 2.
6) Refine gas grid if necessary, or else go to step 8.
7) Go to step 4.
8) Problem converged.

In short, $\dot{m}$ is solved by using a shooting method for the initial boundary-value problem in the two-phase region to give the first-order boundary conditions and to match the second-order boundary conditions of the finite difference boundary-value problem in the gas region. Most of the CPU time is consumed in solving the gas-phase equations. The condensed-phase region solves in seconds, whereas the gas phase can take from minutes to hours depending on the initial guess and the coarseness of the grid. Once the gas region has converged for the first time, all future calculations usually go relatively fast.

Model Inputs

The computer code requires thermodynamic properties, transport properties, and kinetic mechanisms for both the gas- and two-phase regions. There is a lot of scatter in the literature for some property values. This section will discuss the inputs used for RDX. Thermodynamic and transport properties for the gas-phase species were taken from the Chemkin format databases accompanying the August 1995 version of the RDX Yetter mechanism.[16]

RDX Thermodynamic and Physical Properties

The thermodynamic and physical properties used in the model for RDX are listed in Table 1. Because most propellants begin rapid decomposition at or near their melting point, there are very few data for the liquid phase properties. Often liquid property data must either be estimated or extrapolated from the solid property data. Liquid heat capacity, liquid thermal conductivity, and liquid vapor pressure were the least certain

Table 1 Thermodynamic and physical properties of RDX solid and liquid used in model

Property	Value	Reference	Comments
ΔH_fRDX$_{solid}$, 298 K	14.67 kcal/mole	Kubota[17]	——
c_p, solid	0.0389 + 0.000703T, cal/g K	Shoemaker et al.[18]	Curve fit of Shoemaker's data[18]
Thermal condition, solid	4.18×10^{-4} cal/g K	Kubota[17]	——
Solid density	1.806 g/cm^3	Boggs[19]	——
T_{melt}	478 K	Hall[20]	——
ΔH_{fus}	8.51	Boggs[19]	——
c_p, liquid	0.0389 + 0.000703T, cal/gK	——	Assume same as solid
Thermal condition, liquid	8.0×10^{-4} cal/cm s K	——	Estimated
Liquid density	1.806 g/cm^3	——	Assume same as solid
Vapor pressure	10^[11.87−5850/T(K)], torr	Edwards[21]	Chosen because it gave the best model results

Table 2 RDX property values found in the literature

Property	Value	Source	Comments
Heat capacity, cal/g K	0.0389 + 0.000703T	Shoemaker et al.[18]	Measured from pressed RDX crystals
	0.269 at 298 K	Parr and Hanson-Parr[22]	——
	0.3	Beckstead[23]	Listed for HMX, model
	0.35	Brewster et al.[24]	Model
		Li et al.[25]	
	0.45 at 473 K	BenReuven and Caveny[26]	——
Density, g/cm^3	1.82	Kubota[17]	——
	1.806	Boggs[19]	——
	1.75	Flame database[27]	Value given for pellets made from pressed powder
Thermal conductivity, cal/cm s K	4.06×10^{-4}	Shoemaker et al.[18]	Measured from pressed RDX crystals
	1.75×10^{-4}	Beckstead[23]	Model
	3.0×10^{-4}	Parr[22]	Listed for HMX, model
	5.0×10^{-4}	Brewster et al.[24]	Model
	7.6×10^{-4}	Beckstead[28]	Listed for HMX, model
Vapor pressure, torr			
$\log_{10}(P) = A - B/T$	A = 14.8, B = 6799	Rosen and Dickinson[29]	328–371 K, sublimation pressure
$\log_{10}(P) = A - B/T$	A = 11.87, B = 5850	Edwards[21]	384–412 K, sublimation pressure
$\log_{10}(P) = A - B/T$	A = 10.59, B = 4433	Rodgers[30]	505–520 K, vapor pressure
	$P = 10^{14.4} \cdot \exp(-15{,}850/T)$	Maksimov et al.[31]	329–413 K, sublimation pressure
	$P = 10^{16.89} \cdot \exp(-16{,}143/T)$	Cundall et al.[32]	343–447 K, sublimation pressure
	$P = 10^{11.5} \cdot \exp(-12{,}178/T)$	Yang and Liau[33]	Vapor pressure correlation used in their one-dimensional RDX model

properties. A limited literature search was performed to find values for these properties. The results are shown in Table 2 and are discussed later in more detail.

Although there is a lot of scatter in the reported heat capacity and density data, the model's predictions did not change significantly with these parameters. Only one paper was found that contained experimental thermal conductivity for RDX.[18] These data were for the solid, and for the temperature range explored, it appeared to be nearly constant. All of the other values were given in conjunction with models without referencing their source. Values ranged from 1.75×10^{-4} to 7.6×10^{-4} cal/cm·s·K. We chose a value slightly higher than any of these solid thermal conductivities (8.0×10^{-4} cal/cm·s·K), which enabled our model to correctly predict the melt layer thickness.

Several models are based on the assumption that the primary mechanism by which RDX$_{liquid}$ enters the gas phase is by evaporation rather than decomposition.[4,6] Some experiments fail to show the presence of RDX vapor, but this could be a result of RDX rapidly decomposing before it can be detected.[34] Hanson-Parr and Parr[7] detected RDX vapor near the surface of a burning propellant using uv-visible absorption measurements, but claim that the maximum RDX concentration near the surface is only about 7×10^{16} mole/cm^3. Assuming ideal gas and a temperature of 600 K, this represents a mole fraction of about 0.006 (a value much lower than that predicted by most models). In attempting to model RDX evaporation, the literature was searched for vapor pressure data. Four different correlations of sublimation pressure and one of vapor pressure were found (see Fig. 1).

Logically, the vapor pressure data[30] rather than the sublimation data would seem to be the ones to choose since evaporation is being modeled by assuming vapor–liquid equilibrium. Using Rogers' vapor pressure[30] did not affect any of the model's predictions other than lowering the surface temperature by 50–100 K. The data that gave the most reasonable surface temperature predictions was the sublimation pressure from Edwards.[21] Admittedly, we are extrapolating the given pressure correlation beyond the experimental limits. Considering the inaccuracies and assumptions inherent in the evaporation model and the apparent disagreement between evaporation-dominated models and Parrs' results,[7] we choose to use Edwards' data.[21] If we use Rodgers' vapor-pressure correlation,[30] the model indicates that less than 1% of the RDX decomposes in the two-phase region. With Edwards' data,[21] up to 25% of the RDX is calculated to decompose in the two-phase region.

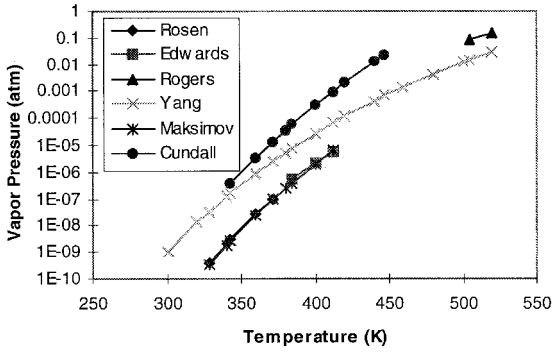

Fig. 1 RDX vapor pressure correlations.

Table 3 Condensed-phase mechanism

Reaction	A	β	E_a
1. RDX(*C*) → $3CH_2O + 3N_2O$	4.88×10^{11}	0.0	36,000
2. RDX(*C*) → $3H_2CN + 3NO_2$	6.5×10^{14}	0.0	45,000
3. $CH_2O + NO_2 \rightarrow NO + CO + H_2O$	802	2.27	13,730
4. RDX(*C*) → RDX_{vapor} (evaporation) Edwards' vapor pressure data			

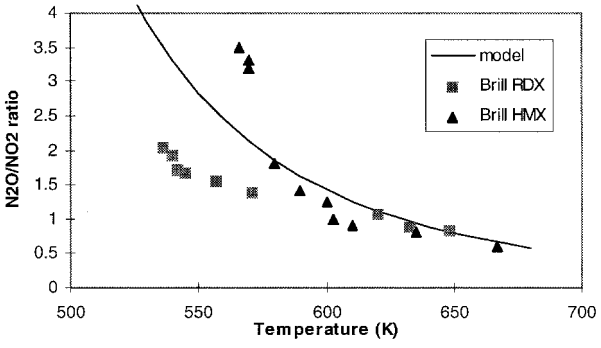

Fig. 2 Condensed phase kinetics.

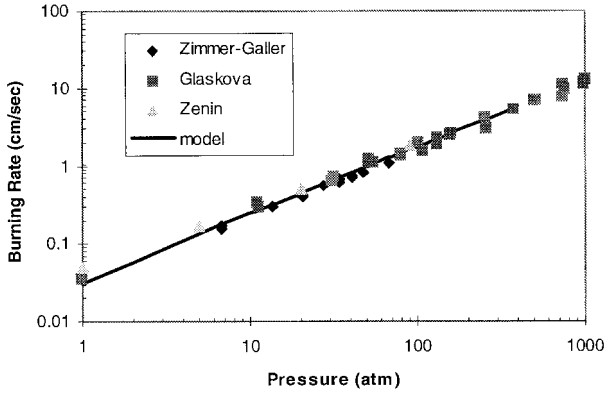

Fig. 3 RDX burning rate (@ T_{init} = 298 K).

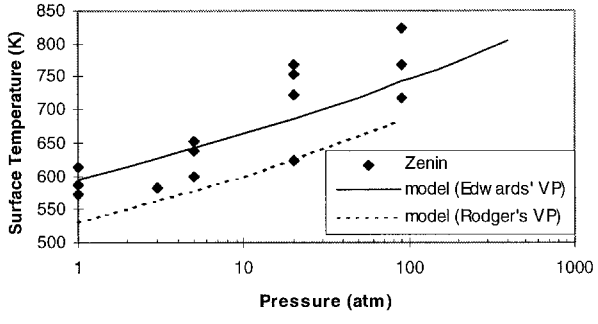

Fig. 4 RDX surface temperature.

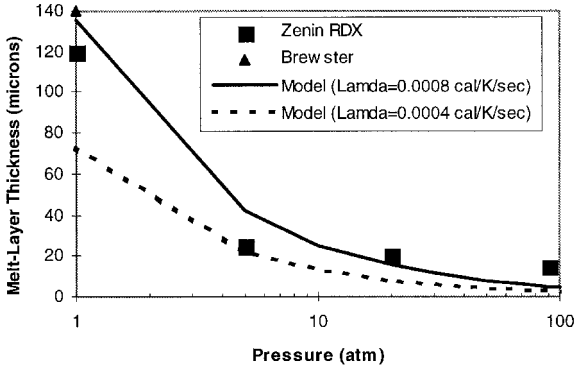

Fig. 5 Melt-layer thickness.

Condensed and Gas Kinetic Parameters

Liau and Yang[6] and Brill[35] presented a summary of the various proposed RDX decomposition mechanisms and such a discussion will not be repeated here. Despite all of the research into RDX decomposition, many questions remain. For this reason, the RDX liquid decomposition mechanism is still semiglobal in nature. The liquid-phase decomposition mechanism is shown in Table 3. This mechanism uses the reaction steps proposed by Thynell et al.,[36] with a few modifications. The pre-exponential constants for reactions 1 and 2 were multiplied by ρ_{rdx}/WT_{RDX} to put the reactions in the right format for the code input. Reaction 2 was divided by two to make the N_2O to NO_2 ratio agree with Brill's measured ratio[35] (see Fig. 2). For reaction 3, Thynell et al.[36] treat CH_2O and NO_2 as dissolved species in the RDX_{liquid}. We choose to treat these species as gas-phase molecules trapped in the bubbles.

The RDX Yetter[16] mechanism (45 species, 231 reactions) was used for the gas-phase mechanism. This mechanism is constantly being improved and results can change with different versions.

Model Predictions

With the input parameters and mechanisms listed earlier, the model agrees very well with most laser- and nonlaser-assisted deflagration data of which the authors are aware. Burning rate as a function of pressure is shown in Fig. 3. Calculations were performed between 1–400 atm. Recent changes in Yetter's RDX gas-phase mechanism[16] have improved agreement between model predictions and experimental burning rate measurements at higher pressures (>70 atm). Several models (including this one) failed to accurately predict burning rate at high pressures using older versions of Yetter's RDX gas-phase mechanism.[16]

Zenin[37] recently reported the surface temperature of burning RDX as a function of pressure. Using Edward's sublimation pressure,[21] the model was able to agree fairly well with Zenin's measured results[37] (see Fig. 4). Higher vapor pressure correlations (like the one used by Liau and Yang[6] or Rodgers[30]) caused the model to underpredict the surface temperature. Changes to burning rate predictions caused by using these different vapor pressure correlations were insignificant. Zenin[37] also reported melt-layer thickness at four different pressures. The melt-layer thickness was very dependent upon the assumed liquid thermal conductivity. Figure 5 shows the predictions using the value of thermal conductivity that we determined and the value of 4.06×10^{-4} cal/cm s (experimentally measured for solid RDX).

σ_p as defined by

$$\sigma_p = \left[\frac{\partial\, \ell n(r_b)}{\partial T_i}\right]_p \tag{19}$$

was also calculated and compared to experimental data by Atwood.[38] The results are shown in Fig. 6. The calculations fall within the uncertainty of the experimental data but are lower than those predicted by the model of Liau and Yang.[6]

Korobeinichev[39] measured species mole fractions in an RDX flame (at 0.5 atm) as a function of distance from the surface.

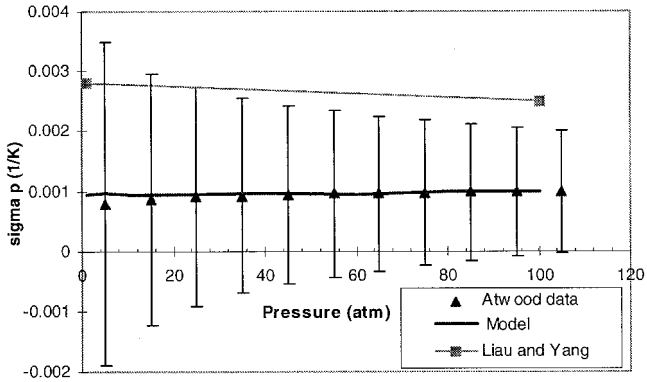

Fig. 6 Temperature sensitivity.

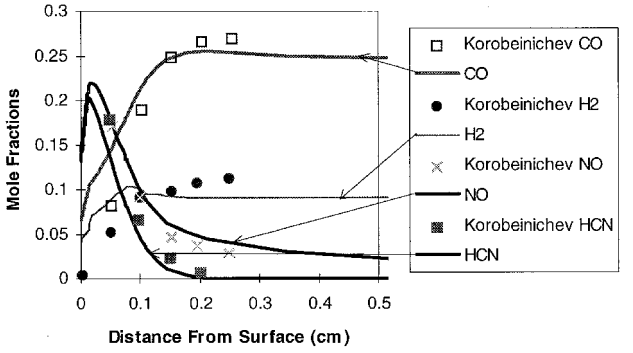

Fig. 7 HCN, NO, H_2, and CO concentration profiles.

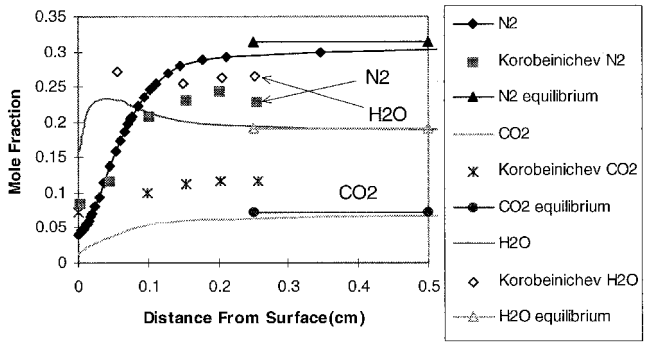

Fig. 8 N_2, H_2O, and CO_2 concentration profiles.

His measurements are compared to those predicted by the model in Figs. 7 and 8. There is good agreement between the experimental data and the predicted values for HCN, NO, H_2, and CO (see Fig. 7). The agreement is not as good for N_2, H_2O, and CO_2 (Fig. 8). The experimental data do not seem to be approaching the equilibrium concentrations, but the calculated concentrations are. If the experimental data are scaled so that they approach the equilibrium concentrations, the agreement would be much better. The fact that the experimental data do not approach the appropriate equilibrium values cast some suspicion on the accuracy of the data.

Hanson-Parr and Parr[7] have done extensive studies of the RDX laser-assisted flame structure. These data are very valuable in verifying the model and mechanisms. The laser flux to the surface increases the deflagration rate and extends the flame structure, giving more space for diagnostic measurements. The experiment is at least two dimensional because the strands of propellant are surrounded by air, and the laser flux intensity is a function of radius. Most monopropellant models with detailed kinetics are one dimensional, but can be made to approximate the two-dimensional characteristics by 1) allowing the flame cross-sectional area to expand as a function of distance from the propellant surface and 2) assuming an average laser flux for the whole surface. Parr and Hanson-Parr[22] quantified the velocity field of the RDX gas flame using particle velocimetry imaging. The following information was used to determine the area expansion expression:

1) The cross-sectional area of the entire flame expands by a factor of 5 between the surface and 5 mm above the surface.[22]

2) The centerline velocity is approximately constant at 550 cm/s.[7]

3) The measured surface regression rate was in the range of 0.06–0.09 cm/s.[22]

4) The radial component of the velocity vectors near the centerline was much smaller than those near the edge of the sample[22] (the center of the flame may not have expanded as much at the entire flame).

5) The length of the measured dark zone is approximately 0.12 cm.

6) The experimentally determined temperature profile was used.[7]

To determine the correct area expansion for use in the model we first fixed the experimentally determined temperature profile in the gas phase and increased the modeled laser flux until the deflagration rate was 0.075 cm/s (average of 0.06 and 0.09 cm/s measured values). If we let the area expand by a factor of 5, the centerline velocity was approximately 125 cm/s (much lower than 550 cm/s). For the centerline velocity to be approximately 500 cm/s, the area could only expand by a factor of 2.4. The laser flux, location of area expansion, and rate of area expansion were then optimized to make the best agreement between the experimental temperature profile and the model's predicted profile. We justified the use of optimization to match the experiment because we were more interested in

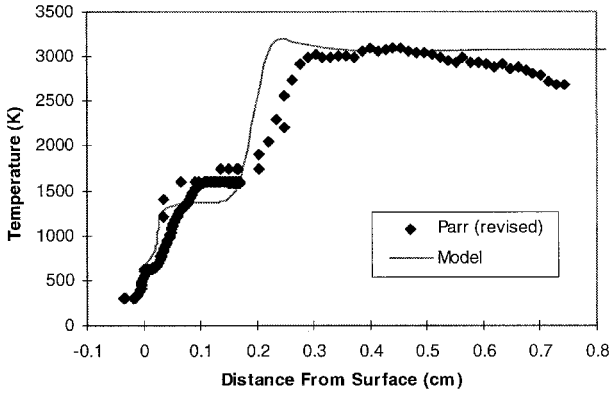

Fig. 9 Laser-assisted temperature profile (1 atm).

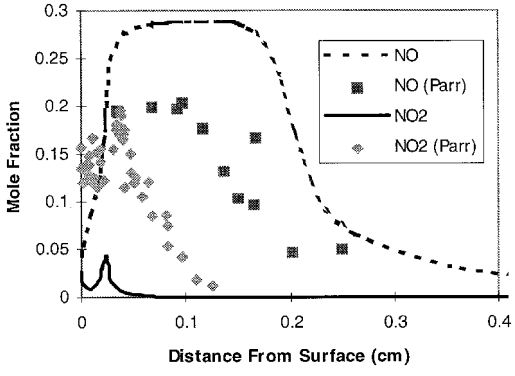

Fig. 10 Laser-assisted NO and NO_2 mole fractions.

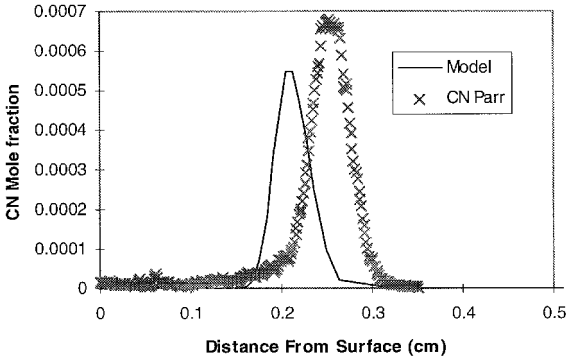

Fig. 11 CN mole fraction.

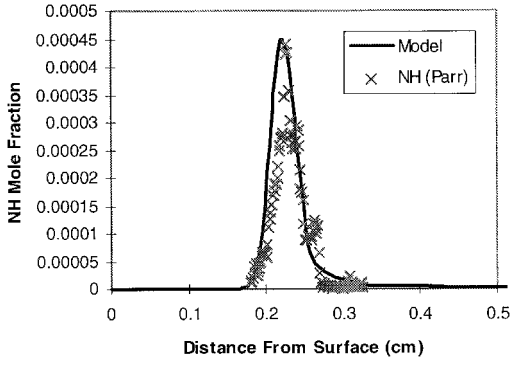

Fig. 12 NH mole fraction.

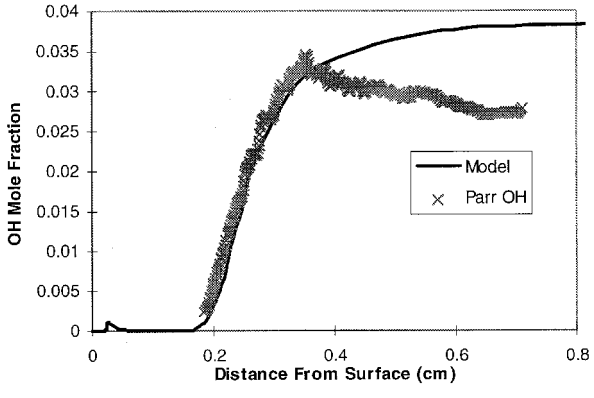

Fig. 13 OH mole fraction.

comparing species concentration profiles than modeling the details of experiment. The optimal area expansion correlation was

$$\text{area} = \begin{cases} 1\ \text{cm}^2 & x < 0.13\ \text{cm} \\ \dfrac{2.4-1}{0.5-0.13}\cdot(x-0.13)+1\ \text{cm}^2 & 0.13 \le x \le 0.5\ \text{cm} \\ 2.4\ \text{cm}^2 & x > 0.5\ \text{cm} \end{cases} \tag{20}$$

An average laser flux of 150 W/cm^2 input to the model gave a calculated surface regression rate of 0.086 cm/s. According to the heat flux-regression rate correlation[22] the laser would have to be set to 283 W/cm^2 to get this burning rate. Therefore, according to the model, the propellant surface is receiving only about 50% of the peak laser flux. Prasad et al.[10] make a similar assumption with their model and postulate that this is because of the Gaussian distribution of the incident laser flux. Because of the uncertainty in the area expansion and nonuniformity of the laser beam we felt that further model complexity (such as in-depth absorption of the laser flux) was not warranted.

The measured and modeled temperature profiles are shown in Fig. 9. (Note: Hanson-Parr and Parr[7] recently reanalyzed their original data and have found an alternate interpretation of their results that gives a higher flame temperature.[22] Previously, their flame temperature was around 2600 K). The agreement in the calculated temperature profile is reasonable, considering the differences between the model and experiment. The experiment shows, and the model predicts, a flame temperature slightly above the adiabatic flame temperature (2925 K) because of the added energy from the laser. There is also good qualitative agreement between most of the species (except NO_2 and NO) concentration profiles and the model's predictions (see Figs. 10–13). It should be noted that the Parrs show that the NO_2 mole fractions decrease with decreasing laser flux.[7] Extrapolating this trend to zero flux gives a scaling factor of 0.29.[22] The fact that the predicted NO_2 appears to be low may not be a problem with the mechanism, but with our inability to model the experiment accurately.

The mole fractions profiles of the major species are shown in Fig. 14 for the laser-assisted case showing the details of the dark zone. The primary flame chemistry in general terms consists of RDX, CH_2O, $N_2O \rightarrow$ HCN, NO, CO, H_2O. The reactions then stall because of the relative stability of NO until there is enough energy for the secondary flame to ignite. The secondary flame chemistry in general terms consists of NO, HCN, $N_2O \rightarrow N_2$, CO, H_2.

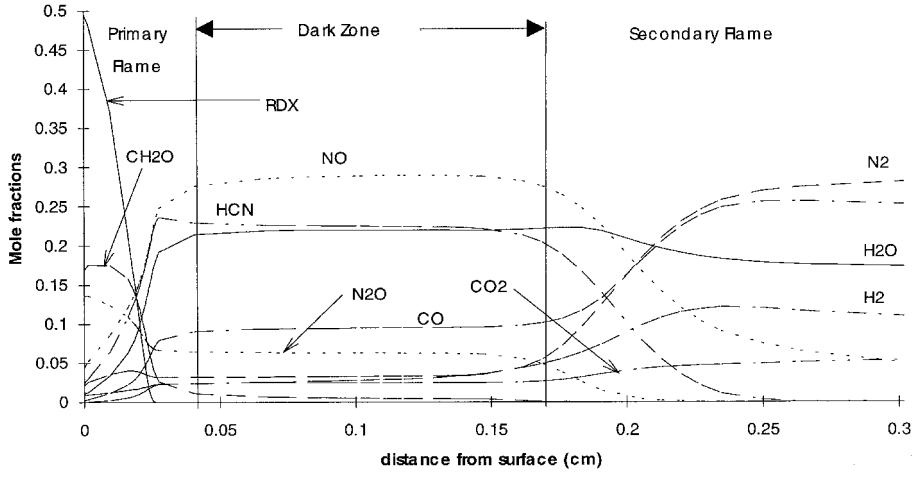

Fig. 14 Calculated laser-assisted mole fraction profiles of major species.

Conclusions

A one-dimensional steady-state monopropellant combustion model has been developed and tested using RDX as the verification or test propellant. With the model inputs given previously, it does a reasonably good job in predicting burning rate (as a function of pressure and initial temperature), surface temperature (as a function of pressure), and melt-layer thickness (as a function of pressure). Predicted species profiles agree well with both laser- and nonlaser-assisted experimental measurements. The major weaknesses of the model occur in the region near the surface. The evaporation–condensation rate calculations, vapor–pressure correlations, liquid thermophysical properties, and the global, condensed-phase mechanism need further study. The model can predict accurate surface temperature data only when using sublimation pressure data rather than vapor pressure data. Other calculated results do not appear to be strong functions of vapor pressure. Unlike other calculated values, melt-layer thickness is a strong function of liquid thermal conductivity. Because no RDX liquid thermal conductivity data could be found in the literature, a value of 8.0×10^{-4} cal/cm·s·K was estimated (about two times the measured solid value). This enabled the model's predicted melt-layer thickness to agree with experimental data by Zenin.[37] The model was also able to match with the Parrs' laser-assisted temperature and species concentration profile data[7] by mimicking the two dimensionality of their experiment with area expansion and averaged laser intensity. The laser increases the advection and thus spreads out the chemical reactions. This effect appears as a two-stage flame or a dark zone in both the experiment and the model.

Acknowledgments

This work was funded by the Air Force Office of Scientific Research under Contract AFOSR F496209-93-1-0430; their support is appreciated.

References

[1]Ben-Reuven, M., Caveny, L. H., Vichnevetsky, R. J., and Summerfield, M., "Flame Zone and Subsurface Reaction Model for Deflagrating RDX," *16th Symposium on Combustion*, The Combustion Inst., Pittsburgh, PA, 1976, pp. 1223–1233.

[2]Ermolin, N. E., Korobeinichev, O. P., Kuibida, L. V., and Fomin, V. M., "Study of the Kinetics and Mechanism of Chemical Reactions in Hexogen Flames," *Fizika Goreniya i Vzryva*, Vol. 22, No. 5, 1986, pp. 544–553.

[3]Hatch, R. L., "Chemical Kinetics Modeling of HMX Combustion," *24th JANNAF Combustion Meeting*, Vol. 1, Chemical Propulsion Information Agency, 1987, pp. 383–391 (Paper 476).

[4]Melius, C. F., "Thermochemical Modeling: II. Application to Ignition and Combustion of Energetic Materials," *Chemistry and Physics of Energetic Materials*, Kluwer, Dordrecht, The Netherlands, 1990, pp. 51–78.

[5]Yetter, R. A., Dryer, F. L., Allen, M. T., and Gatto, J. L., "Development of Gas-Phase Reaction Mechanisms for Nitramine Combustion," *Journal of Propulsion and Power*, Vol. 11, No. 4, 1995, pp. 683–697.

[6]Laiu, Y.-C., and Yang, V., "Analysis of RDX Monopropellant Combustion with Two-Phase Subsurface Reactions," *Journal of Propulsion and Power*, Vol. 11, No. 4, 1995, pp. 729–739.

[7]Hanson-Parr, D., and Parr, T., "RDX Laser-Assisted Flame Structure," *31st JANNAF Combustion Meeting*, Vol. 2, Chemical Propulsion Information Agency, 620, Columbia, MD, 1994, pp. 407–423.

[8]Bizot, A., Beckstead, M. W., and Korobeinichev, O. P., "A Model for HMX Propellant Combustion," *Flame Structure*, Novosibirsk, Russia, 1991, pp. 230–235.

[9]Li, S. C., and Williams, F. A., "Nitramine Deflagration: A Reduced Chemical Mechanism for the Primary Flame," AIAA Paper 94-3041, June 1994.

[10]Prasad, K., Yetter, R., and Smooke, M., "An Eigenvalue Approach for Computing the Burning Rates of RDX Propellant," Fall Meeting of the Eastern States Section, The Combustion Inst., Pittsburgh, PA, Oct. 1994.

[11]Brown, P. N., Hindmarsh, A. C., and Byrne, G. D., "DVODE," Double Precision Variable Coefficient Ordinary Differential Equation Solver, Lawrence Livermore National Lab., Aug. 1992.

[12]Kee, R. J., Rupley, R. M., and Miller, J. A., "Chemkin-II: A Fortran Chemical Kinetics Package for the Analysis of Gas Phase Chemical Kinetics," Sandia Rept., SAND89-8009B·UC-706, April 1992.

[13]Kee, R. J., Dixon-Lewis, G., Warnatz, J., Coltrin, M. E., and Miller, J. A., "A Fortran Computer Code Package for the Evaluation of Gas-Phase Multicomponent Transport Properties," Sandia Rept., SAND86-8246·UC-401, July 1992.

[14]Margolis, S. B., and Williams, F. A., "Influences of Two-Phase Flow in the Deflagration of Homogeneous Solids," *Combustion and Flame*, Vol. 67, No. 2, 1987, pp. 249–258.

[15]Kee, R. J., Grear, J. F., Smooke, M. D., and Miller, J. A., "A Fortran Program for Modeling Steady Laminar One-Dimensional Premixed Flames," Sandia Rept., SAND85-8240·UC-401, April 1992.

[16]Prasad, K., Yetter, R., and Smooke, M., "An Eigenvalue Method for Computing the Burning Rates of RDX Propellants," *32nd JANNAF Combustion Meeting*, Vol. 1, Chemical Propulsion Information Agency, 638, Columbia, MD, 1995, pp. 69–84; also Ref. 5.

[17]Kubota, N., "Survey of Rocket Propellants and Their Combustion Characteristics," *Fundamental of Solid-Propellant Combustion*, edited by K. K. Kuo and M. Summerfield, Vol. 90, Progress in Astronautics and Aeronautics, AIAA, New York, 1984, pp. 1–52.

[18]Shoemaker, R. L., Stark, J. A., and Taylor, R. E., "Thermophysical Properties of Propellants," *High Temperatures-High Pressures, ETPC Proceedings*, Vol. 17, Pion, UK, 1985, pp. 429–435.

[19]Boggs, T. L., "The Thermal Behavior of Cyclotrimethylenetrinitramine (RDX) and Cyclotetramethylenetetranitramine (HMX)," *Fundamentals of Solid Propellant Combustion*, Vol. 90, Progress in Astronautics and Aeronautics, AIAA, New York, 1984, pp. 121–175.

[20]Hall, P. G., "Thermal Decomposition and Phase Transitions in Solid Nitramines," *Transactions of the Faraday Society*, Vol. 67, Pt. 2, 1971, pp. 556–562.

[21]Edwards, G., "The Vapour Pressure of Cyclo-Trimethylene-Trinitramine (Cyclonite) and Pentaerythritol-Tetranitrate, *Transactions of the Faraday Society*, Vol. 49, 1953, pp. 152–154.

[22]Parr, T., and Hanson-Parr, D., "RDX, HMX and XM39 Self-Deflagration Flame Structure," *32nd JANNAF Combustion Meeting*, Vol. I, Chemical Propulsion Information Agency, 631, Columbia, MD, 1995, pp. 429–438; also Ref. 7.

[23]Beckstead, M. W., "Modeling AN, AP, HMX, and Double Base Monopropellants," *26th JANNAF Combustion Meeting*, Vol. 4, Chemical Propulsion Information Agency, 1989, pp. 255–268 (Paper 524).

[24]Brewster, M. Q., Zebrowski, M. A., Schroeder, T. B., and Son, S. F., "Unsteady Combustion Modeling of Energetic Solids," AIAA Paper 95-2859, July 1995.

[25]Li, S. C., Williams, F. A., and Margolis, S. B., "Effects of Two-Phase Flow in a Model for Nitramine Deflagration," *Combustion and Flame*, Vol. 80, No. 2, 1990, pp. 329–349.

[26]BenReuven, M., and Caveny, L. H., "HMX Deflagration and Flame Characterization," Vol. II, Thiokol Corp., AFRPL-TR-79-94, Huntsville, AL, Oct. 1980.

[27]Fogelzang, A. E., "Flame," Combustion of Explosives and Propellants Database, Version 2.43, Moscow, Russia, 1994.

[28]Beckstead, M. W., "A Propellant Ignition Code for Moter Applications," *31st JANNAF Combustion Meeting*, Vol. 2, Chemical Propulsion Information Agency, 1994, pp. 163–180 (Paper 620).

[29]Rosen, J. M., and Dickinson, C., "Vapor Pressures and Heats of Sublimation of Some High Melting Organic Explosives," *Journal of Chemical and Engineering Data*, Vol. 14, No. 1, 1969, pp. 120–124.

[30]Rogers, R. N., "Determination of Condensed Phase Kinetic Constants," *Thermochimica Acta*, No. 9, 1974, pp. 444–446.

[31]Maksimov, Y. Y., Apal'kova, V. N., Braverman, O. V., and Solov'ev, A. I., "Kinetics of Thermal Decomposition of Cyclotrimethylenetrinitramine and Cyclotetramethylene-Tetranitramine in Gas Phase," *Russian Journal of Physical Chemistry*, Vol. 59, 1985, pp. 201–204.

[32]Cundall, R. B., Palmer, T. F., and Wood, C. E. C., "Vapour Pressure Measurements of Some Organic Explosives," *Journal of the Chemical Society, Faraday Transactions I*, Vol. 74, 1978, pp. 1339–1345.

[33]Yang, V., and Liau, Y., "A Time-Accurate Analysis of RDX Monopropellant Combustion with Detailed Chemistry," *32nd JANNAF Combustion Meeting*, Vol. I, Chemical Propulsion Information Agency, 638, 1995, pp. 57–67; also Ref. 6.

[34]Tang, C.-J., Lee, Y., and Litzinger, T. A., "A Study of Gas-Phase Processes During the Deflagration of RDX Composite Propellants Using a Triple Quadrupole Mass Spectrometer," *31st JANNAF Combustion Meeting*, Vol. 2, Chemical Propulsion Information Agency, 1994, pp. 425–437 (Paper 620).

[35]Brill, T. B., "Multiphase Chemistry Considerations at the Surface of Burning Nitramine Monopropellants," *Journal of Propulsion and Power*, Vol. 11, No. 4, 1995, pp. 740–751.

[36]Thynell, S., Gongwer, P. E., and Brill, T. B., "Modeling of Thermal Response of Filament Used in T-Jump Experiment," *31st JANNAF Combustion Meeting*, Vol. 2, Chemical Propulsion Information Agency, 1994, pp. 221–232 (Paper 620).

[37]Zenin, A., "HMX and RDX: Combustion Mechanism and Influence on Modern Double-Base Propellant Combustion," *Journal of Propulsion and Power*, Vol. 11, No. 4, 1995, pp. 752–758.

[38]Boggs, T. L., Atwood, A. I., Curran, P. O., Parr, T. P., Hanson-Parr, D., Paull, D., Wiknich, J., and Price, C. F., "The Pressure and Temperature Sensitivity of Burning Rates of Solid Propellant Ingredients," U.S. Naval Air Warfare Center, Weapons Div., China Lake, CA, 1995.

[39]Korobeinichev, O. P., "Dynamic Flame Probe Mass Spectrometry and Condensed-System Decomposition," *Fizika Goreniya i Vzryva*, Vol. 23, No. 5, 1987, pp. 64–76.